ACS APPLIED MATERIALS & INTERFACES
Letter
www.acsami.org

Complex Logic Functions Implemented with Quantum Dot Bionanophotonic Circuits

Jonathan C. Claussen,[†,⊥] Niko Hildebrandt,[#] Kimihiro Susumu,[‡,∥] Mario G. Ancona,[§] and Igor L. Medintz*,[†]

[†]Center for Bio/Molecular Science and Engineering, Code 6900; [‡]Optical Sciences Division, Code 5600; [§]Electronics Science and Technology Division, Code 6876; U.S. Naval Research Laboratory, Washington, D.C. 20375, United States

[⊥]College of Science, George Mason University, Fairfax, Virginia 22030, United States

[#]NanoBioPhotonics, Institut d'Electronique Fondamentale, Université Paris-Sud, 91405 Orsay Cedex, France

[∥]Sotera Defense Solutions, Annapolis Junction, Maryland 20701, United States

Supporting Information

ABSTRACT: We combine quantum dots (QDs) with long-lifetime terbium complexes (Tb), a near-IR Alexa Fluor dye (A647), and self-assembling peptides to demonstrate combinatorial and sequential bionanophotonic logic devices that function by time-gated Förster resonance energy transfer (FRET). Upon excitation, the Tb-QD-A647 FRET-complex produces time-dependent photoluminescent signatures from multi-FRET pathways enabled by the capacitor-like behavior of the Tb. The unique photoluminescent signatures are manipulated by ratiometrically varying dye/Tb inputs and collection time. Fluorescent output is converted into Boolean logic states to create complex arithmetic circuits including the half-adder/half-subtractor, 2:1 multiplexer/1:2 demultiplexer, and a 3-digit, 16-combination keypad lock.

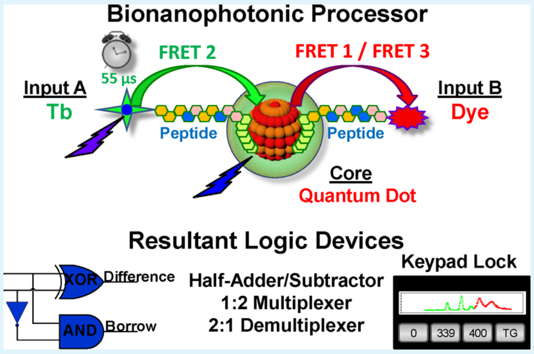

KEYWORDS: *Förster resonance energy transfer (FRET), biocomputing, molecular logic, quantum dot, terbium, lanthanide*

1. INTRODUCTION

Since their introduction, molecular logic devices (MLDs) have been intriguing for their potential to mimic functions of silicon circuitry at molecular scales.[1−6] Current research in this area now focuses on incorporating chemical or biologically active components to augment the sensing, reconfiguration, flexibility and signal transduction capabilities of such devices.[5,7−18] Although this work has broadened the utility of MLDs, their potential remains severely circumscribed because of the challenge in achieving input/output (I/O) signal compatibility that allows one gate to drive another as is required for more sophisticated circuits.[4,5,19] In the face of this roadblock, we show how it is still possible to implement fairly complex functions using parallel, single-stage MLD logic based on functionalized semiconductor quantum dots.

We previously utilized semiconductor quantum dots (QDs) self-assembled with terbium III complex- (Tb) and Alexa Fluor 647- (A647) dye-labeled peptides to demonstrate both biosensors[20,21] and single-input, double-output bionanophotonic logic gates (e.g., AND/OR gates).[22] With a millisecond lifetime, the Tb serves as a memory element capable of "storing/carrying" information while directly sensitizing the QDs and indirectly sensitizing any downstream FRET acceptors attached to the QD. Critically, the delayed nature of the Tb sensitization allows it to be monitored in a time-gated manner that adds a unique extra dimension to the signal space. In these devices, the QD acts as a supramolecular nuclei that orchestrates the self-assembly of the constructs while providing numerous FRET benefits (i.e., conjugation with multiple donor or acceptor molecules in a centrosymmetric fashion, selective/predefined tuning of FRET efficiency, etc.) that have been extensively detailed in recent publications.[23−31] Here, we demonstrate that the same functional architecture of our earlier work is much richer computationally than we had hypothesized and is capable of implementing significantly more complex logic functions. As in ordinary digital logic, these QD-based "circuits" are built up from simpler logic elements; however, we demonstrate that these "circuits" can be produced from optically interrogated, parallel single-stage combinations of QD/dye-peptide bioconjugates in lieu of concatenated networks of individual logic gates. We build upon our initial work and demonstrate how the same functional architecture can exploit ratiometric assembly to QDs along with time-dependent variable output to provide far more complex, combinatorial and sequential bionanophotonic logic devices (BLDs) that utilize multiple logic gates to produce complex combinatorial circuits (half-adder, half-subtractor, 2:1 multiplexer, 1:2 demultiplexer) and sequential logic (3-digit, 16-combination keypad lock).

Received: October 22, 2013
Accepted: December 6, 2013
Published: December 19, 2013

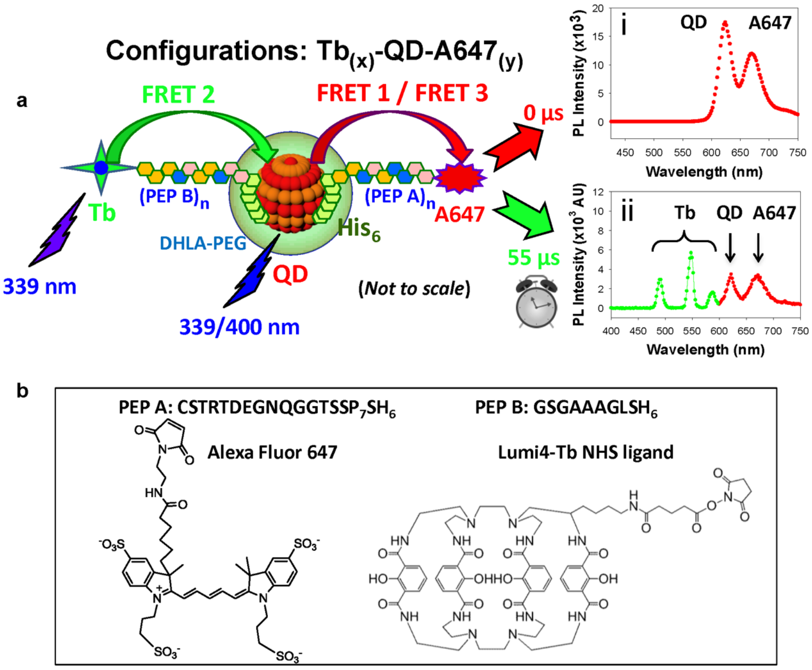

Figure 1. Logic device schematic. (a) Logic device architecture consisting of terbium(III) complex (Tb, left green) and Alexa Fluor 647 dye (A647, right red) conjugates co-assembled around a central quantum dot (QD, center red) via peptides PEB B and PEP A, respectively. The peptides self-assemble to the QDs in an oriented manner via $(\mathrm{His})_6$-driven metal affinity coordination. Relative Tb/A647 valence per QD is abbreviated as $\mathrm{Tb}_{(x)}$-QD-$\mathrm{A647}_{(y)}$. Multiple FRET processes originate from the QD or the Tb depending upon excitation wavelength. 400 nm excites the QD, which in turn emits or sensitizes the A647 by FRET 1; the QD/A647 donor/acceptor emission is monitored immediately with no time-delay (0 μs). 339 nm light excites both the Tb and QD, the QD emits or sensitizes the A647 by FRET 1. A 55 μs time-delay allows the QD to relax and the long-lifetime Tb to sensitize the QD by FRET 2, which in turn, sensitizes the A647 by FRET 3. Representative spectra for both processes are shown in panels i, ii, respectively. Relevant photophysical and FRET properties are as follows. QD: $\varepsilon_{610\ \mathrm{nm}} = 5.5 \times 10^5\ \mathrm{M}^{-1}\ \mathrm{cm}^{-1}$, $\lambda_{\mathrm{em.max}} = 625$ nm, quantum yield $\Phi \approx 0.6$, PL lifetime $\tau \approx 50$ ns. Tb: $\lambda_{\mathrm{abs.max}} = 339$ nm, $\varepsilon_{\mathrm{max}} = 26\,000\ \mathrm{M}^{-1}\ \mathrm{cm}^{-1}$, $\lambda_{\mathrm{em.max.}} = 490/550/585/620$ nm, $\Phi \approx 0.60$, $\tau \approx 2.6$ ms. A647: $\lambda_{\mathrm{abs.max}} = 650$ nm, $\varepsilon_{\mathrm{max}} = 89\,000\ \mathrm{M}^{-1}\ \mathrm{cm}^{-1}$, $\lambda_{\mathrm{em.max}} = 670$ nm, $\Phi \approx 0.33$, $\tau \approx 1$ ns. Förster distances (R_0): R_0(FRET 1 Tb→QD) = 10.1 nm, R_0(FRET 2/FRET 3 QD→A647) = 7.5 nm. Note: the Tb is not excited at 400 nm. (b) Peptide sequences and chemical structures of A647 and the Lumi4 ligand that chelates the Tb^{3+} ion.

2. EXPERIMENTAL METHODS

Materials. BLDs were self-assembled from 625 nm emitting CdSe/ZnS QDs solubilized with poly(ethylene glycol) PEG-appended dihydrolipoic acid, and conjugated with one of two peptides (Biosynthesis, Lewisville, Texas), see Figure 1. PEP A-A647 was labeled with Alexa Fluor 647-maleimide at the *N*-terminal cysteine residue while PEP B–Tb was *N*-terminally labeled with *N*-hydroxysuccinimide ester Lumi4 Tb. Preparation of these materials has been described in detail elsewhere.[20−22,32−35]

Device Assembly. QD–peptide conjugates were prepared at 45 nM by adding QD to a prediluted solution of the desired equivalents of PEP A–A647 and PEP B–Tb in phosphate-buffered saline (PBS, 10 mM phosphate, 137 mM NaCl, 3 mM KCl, pH 7.4) to a final volume of ∼110 μL. Device Tb/A647 is abbreviated as $\mathrm{Tb}_{(x)}$-QD-$\mathrm{A647}_{(y)}$ with x and y indicating the respective valences. Solutions were equilibrated at room temperature for 1–2 h prior to collecting photoluminescence (PL) measurements.[20−22] The QD-based BLDs were assembled using our previous fabrication protocol.[20−22] Ratiometric, spontaneous self-assembly of polyhistidine (His_n)-appended/labeled PEP A-A647/PEP B–Tb to the Zn^{2+}-rich QD surface is used to complete the devices. This process was driven by metal affinity coordination ($K_d^{-1} \sim 1 \times 10^9\ \mathrm{M}^{-1}$) and essentially requires only adding molar ratios of the reactants together.[36−39] In our experience, this process can be extended to DNA terminally modified with a polyhistidine tag (His_n) containing peptide sequences—a process that is more facile and rapid than direct attachment of DNA to QDs via thiol bonding, EDC chemistry to join amine or carboxyl-functionalized DNA, or attaching biotinylated DNA to streptavidin-coated QDs.[40,41] However, using DNA to attach a fluorophore to a QD could change the orientation of the dye during the self-assembly process, which in turn would affect the FRET efficiency of the system. Thus, to circumvent these challenges, we carried out QD–fluorophore labeling with peptides in lieu of DNA.

Photoluminescent Characterization. PL spectra were collected in 96-well microtiter well plates on a Tecan Infinite M1000 dual monochromator multifunction plate reader (Tecan, Research Triangle Park, NC) using a xenon flash lamp source. Immediate (0 μs) spectra acquisition: 400 nm excitation, 400 Hz flash frequency, ∼0 μs delay between flash and acquisition, 40 μs integration time. Time-delayed spectra acquisition (55 μs): 339 nm excitation, 100 Hz flash frequency, 55 μs delay, 1000 μs integration time or as indicated. Note that the photophysical properties and interactions of these materials are complex, and their spectra, relative intensities, and cross-contributions may vary depending upon instrumentation and settings utilized.[20−22,29,42]

3. RESULTS AND DISCUSSION

Photophysical Properties and Logic Function. The fully assembled Tb-QD-A647 constructs reveal three distinct time-varying FRET events, QD→A647, Tb→QD, and Tb→

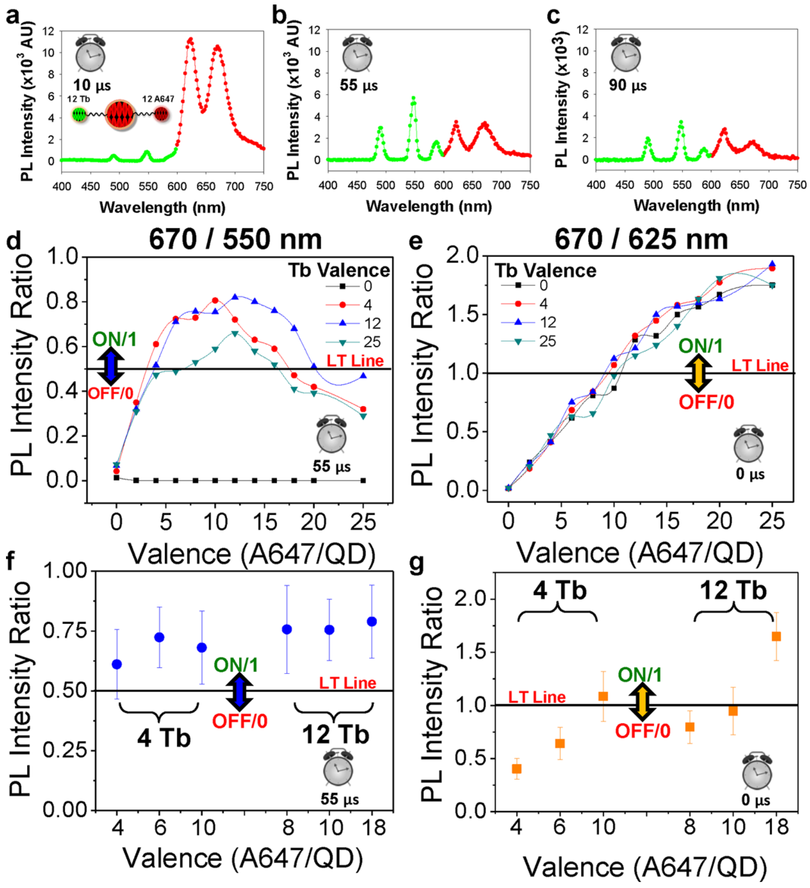

Figure 2. Time-variant PL spectra and conversion into Boolean logic. Representative PL spectra after 339 nm excitation for $Tb_{(12)}$-QD-$A647_{(12)}$ conjugates where the time-delay varies between (a) 10, (b) 55, and (c) 90 µs. (d) Peak PL intensity ratios of A647(670 nm)/Tb(550 nm) acquired 55 µs after 339 nm excitation where Tb to QD valence is held at 0, 4, 12, and 25, whereas A647 to QD valence is varied from 0 to 25 (0, 2, 4, 6, 8, 10, 12, 14, 16, 18, 20, 25). Threshold logic transition (LT) line is set to 0.5. (e) Peak PL intensity ratios of A647(670 nm)/QD(625 nm) for the same construct with the same Tb/A647 valences as in d, acquired immediately (~0 µs) after 400 nm excitation. The LT line is set to 1. (f) Average peak PL intensity ratios for A647(670 nm)/Tb(550 nm) with Tb to QD valence set at 4 and 12 and corresponding A647 to QD valences of 4, 6, 10 and 8, 10, 18, respectively. Sample excited at 339 nm and emission collected with a 55 µs time-delay. Error bars show standard deviation with $n = 6$. (g) Average peak PL intensity ratios for A647(670 nm)/QD(625 nm) with Tb to QD valence set at 4 and 12 and corresponding A647 to QD valences of 4, 6, 10 and 8, 10, 18 respectively. Sample excited at 400 nm and emission collected with 0 µs time-delay. Error bars show standard deviation with $n = 6$.

QD→A647, that we refer to as FRET 1, FRET 2, and FRET 3, respectively (see Figure 1).[20−22] In this configuration, the QD serves as a central switchboard shuttling energy absorbed from UV excitation, or transferred from the Tb, and dispersing it as QD emission or sensitizing the A647 in a toggle-like fashion. Upon 400 nm excitation, the QD alone is initially excited and QD→A647 FRET 1 occurs at <100 ns as revealed in the observation of a QD/A647 donor/acceptor emission spectrum (Figure 1a-i). Upon 339 nm excitation, both QD and Tb are initially excited and FRET 1 again occurs. After sufficient time-delay (~55 µs), the QD relaxes and subsequently accepts Tb→QD FRET 2 sensitization, which, in turn, sensitizes the A647 via Tb→QD→A647 FRET 3 (Figure 1a-ii). The unique combination of absorption/emission, spectral overlap, and excited state lifetimes found in this system enable these three FRET processes as discussed in detail elsewhere.[20−22] Here, our interest is in the effect that distinct BLD inputs (as expressed in A647 and Tb valences, excitation wavelength, and spectral acquisition time) have on post excitation (339/400 nm) PL spectra with or without time delay. Cumulatively, this gives rise to a rich variability in spectra that have temporally-dependent component intensities.

The spectral data are converted into logic gate output by monitoring, for example, the PL intensity ratios of A647(670 nm)/QD(625 nm) and A647(670 nm)/Tb(550 nm) as a function of A647 and Tb valence. Figures 2a−c highlight how the relative intensity ratios evolve over time as the emission lines or spectra associated with Tb (490, 550, and 585 nm in green), QD (625 nm in red), and A647 (670 nm in red) are plotted at 10, 55, and 90 µs. The peak Tb emission lines reach a relative maximum at approximately 55 µs (Figure 2b) and thus a 55 µs time-delay was chosen as the time-gate in subsequent BLD experiments. Plotting the A647/Tb PL intensity ratios acquired at a 55 µs time-delay while varying Tb/A647 valence yields a distinct parabolic profile (Figure 2d) while data obtained from the same constructs monitored as the A647/QD ratio without time-delay provide output that is linear in nature (Figure 2e). The parabolic nature of the former arises from the complex underlying photophysics of the time-gated multi-FRET system.[20−22,29,42] The linear effect is caused by the increasing FRET efficiency of FRET 1 (i.e., QD→A647) with increasing number of A647 dyes conjugated to the central QD (QD PL intensity decreases while A647 PL intensity increases). To convert these PL intensity ratios into Boolean logic "ON"/

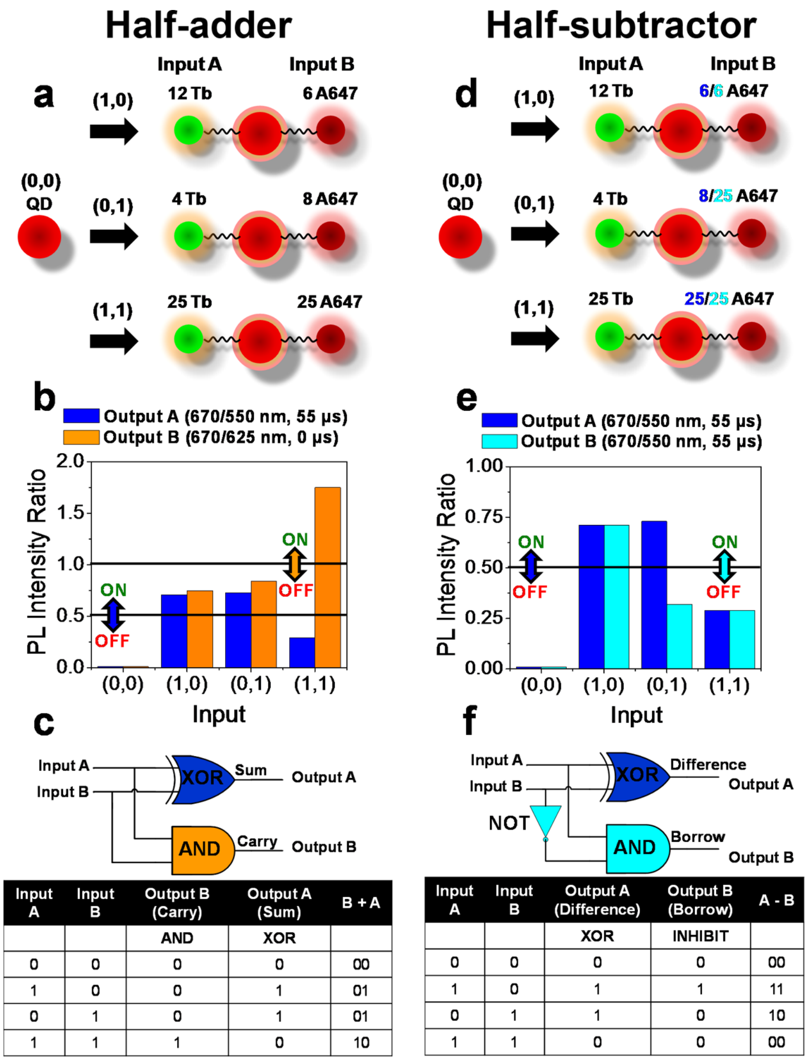

Input A	Input B	Output B (Carry)	Output A (Sum)	B + A
		AND	XOR	
0	0	0	0	00
1	0	0	1	01
0	1	0	1	01
1	1	1	0	10

Input A	Input B	Output A (Difference)	Output B (Borrow)	A - B
		XOR	INHIBIT	
0	0	0	0	00
1	0	1	1	11
0	1	1	0	10
1	1	0	0	00

Figure 3. Half-adder/subtractor. Two-input molecular photonic (a−c) half-adder and (d−f) half-subtractor displaying (a, d) the corresponding functional architecture with Tb (small green sphere) and A647 (small red sphere) valences around the QD (central red sphere) for each input. (d) Note: A647 valence for the XOR and INH gate is shown in dark and light blue, respectively. (b, e) Peak PL intensity ratio of A647(670 nm)/Tb(550 nm) and A647(670 nm)/QD(625 nm) acquired 55 μs (339 nm excitation) and 0 μs (400 nm excitation) after excitation, respectively, where the ratio above 0.5 or 1, respectively, is converted into the Boolean logic state of "ON or 1" and below as "OFF or 0". The corresponding (c, f) circuit diagrams and truth tables where individual gates within the circuits are colored coded to coincide with the corresponding PL intensity ratios that they are generated from.

"OFF" or "0"/"1" values a threshold logic transition (LT) line is established at 0.5 for the A647(670 nm)/Tb(550 nm) time-gated ratio and 1.0 for the A647(670 nm)/QD(625 nm) nongated ratio (Figure 2d−g). Thus, ratio values above the respective LT lines are assigned values of "ON" or "1" while those below are given values of "0" or "OFF". Statistical analysis on the PL intensity ratio outputs ($n = 6$) showed ~0.15 average standard deviations (Figure 2f, g), confirming that inputs needed to be chosen so their corresponding PL intensity ratio values were statistically defined above/below the LT line. For example, when the Tb to QD and A647 to QD valence is set to 4 and 10 respectively and the PL is monitored in a time-gated fashion, the LT line falls within one standard deviation from the 670/620 nm PL intensity ratio mean and thus could make the logical output ambiguous (see Figure 2f). Therefore, in this work, we choose Tb-QD-A647 systems with Tb to QD and A647 to QD valences that yield the demonstrated resultant logic within a confidence interval of 95%, assuming the PL intensity ratio values are normally distributed.

Half-Adder and Half-Subtractor. Arithmetic that requires binary addition of two digits (0 + 0 = 0, 0 + 1 = 1, 1 + 0 = 1, 1 + 1 = 10) can be carried out via a half-subtractor circuit. Because the sum of two binary numbers can be larger than either number (1 + 1 = 10, which corresponds to 2 in base-10) the half-adder provides a "carry" digit (0 + 0 = 0 + 1 = 1 + 0 = 0 and 1 + 1 = 1) and "sum" digit (0 + 0 = 1 + 1 = 0 and 0 + 1 = 1 + 0 = 1). Our QD-based half-adder circuit is created by processing two parallel operating logic gates, the XOR (exclusive OR) and AND gates from the same Tb-QD-A647 system (Figure 3a−c). The half-adder dichotomy is achieved by utilizing the $\text{Tb}_{(x)}$-QD-$\text{A647}_{(y)}$ inputs and distinct PL intensity ratios (i.e., 670/550 and 670/625 nm) with/without time-gating as outputs to create XOR/AND logic. The non-gated AND function produces a "1" output when only both inputs are present and generates the carry digit (first of the two output digits) for the half-adder. The time-gated XOR gate acts as a comparator that produces a "1" output when one and only one input is present and generates the sum digit (second of the two output digits) for the half-adder. Thus, in the half-adder circuit, for example, the presence of both inputs (1, 1) produces an output digit of "1" followed by a digit "0" to yield (1 + 1 = 10). The inputs to this QD-based half-adder are coded in the QD valences, with Inputs A and B having the following definitions: (0,0) QD alone; (1,0) $Tb_{(12)}$-QD-$A647_{(6)}$; (0,1) $Tb_{(4)}$-QD-$A647_{(8)}$; and (1,1) $Tb_{(25)}$-QD-$A647_{(25)}$ (Figure 3a−c). The spectra corresponding to these configurations can be found in the Supporting Information. Output A for the half-adder consists of the PL ratio A647(670 nm)/Tb(550 nm), whereas output B is the ratio A647(670 nm)/QD(625 nm) acquired 55 and 0 μs after excitation, respectively. When the former ratio is above 0.5 or the latter is above 1, the outputs are in the Boolean logic state of "ON or 1" and otherwise are "OFF or 0" (Figure 3b).

The QD-based half-adder utilizes XOR logic that we have previously demonstrated.[22] Such XOR logic remains challenging to produce on the molecular level as both the ground state (0,0) and double input state (1,1) need to be "OFF" or "0"; thus, the complete absence or presence of a biochemical agent is needed to produce the ground and double input state of the half-adder in a potential sensing configuration. Efforts to achieve molecular-based XOR logic include complex hairpin DNA probe confirmations,[43] dye irradiation/excitation at multiple wavelengths,[44] and molecular machine threading/unthreading.[3] Our design bypasses such complexities by utilizing the parabolic nature of the PL intensities acquired with a 55 μs time-delay from excitation; in particular, the parabolic PL profile permits an "OFF" state to be output in response to both the ground (0,0) and double input state (1,1) while being "ON" for the single input states of (1, 0) and (0, 1) (Figure 2d). Furthermore, both the XOR and the AND logic can be realized with identical Tb and A647 valences by monitoring distinct PL ratios at different times. Thus, we are able to generate both the sum and carry digits needed to produce the half-adder without the need to manipulate the Tb-QD-A647 chemical structure.

The QD-based half-subtractor is constructed following a similar protocol (Figure 3d−f). It is capable of binary subtraction of two digits. The half-adder produces a "difference" digit (0 − 0 = 1 − 1 = 0 and 1 − 0 = 0 − 1 = 1) and "borrow" digit (0 − 0 = 1 − 0 = 1 − 1 = 0 and 0 − 1 = 1) because the subtraction of "1" from "0" results in a negative number. We create the half-subtractor by utilizing parallel XOR/INHIBIT (INH) gates (i.e., combination of NOT and AND logic, see circuit diagram Figure 3f) to produce the difference and borrow digits, respectively. The INH or anticoincidence circuit (combines NOT and AND) produces an output of "1" when one and only one input is present. The PL output of the XOR gate is created with the same Tb and A647 inputs of the half-adder monitored at the 670/550 nm PL intensity ratio at a 55 μs time-delay (dark blue numbers for A647 valence in Figure 3d). However, the INH gate of the half-subtractor is created with different A647 inputs: (0, 0) QD alone; (1, 0) $Tb_{(12)}$-QD-$A647_{(6)}$; (0, 1) $Tb_{(4)}$-QD-$A647_{(25)}$; and (1, 1) $Tb_{(25)}$-QD-$A647_{(25)}$ (light blue numbers for A647 valence in Figure 3d). The PL outputs associated with both XOR (dark blue, Figure 3e) and INH (light blue, Figure 3e) gate inputs are obtained by monitoring the PL intensity ratio of A647(670 nm)/Tb(550 nm) 55 μs after excitation with 0.5 as the LT line.

2:1 Multiplexer and 1:2 Demultiplexer. Multiplexers are circuits that act as controlled rotary switches in which any of multiple inputs may be chosen as a single output.[4,45] Our photonic 2:1 multiplexer (0 + 0 = 0; 0 + 1 = 0 or 1; 1 + 0 = 0 or 1; 1 + 1 =1) uses a control input (i.e., select) along with two inputs (input A/B) to choose the output (Figure 4c). Input A and input B contain the states: (0, 0) QD alone without Tb/A647; (1, 0) $Tb_{(12)}$-QD-$A647_{(6)}$; (0, 1) QD $Tb_{(4)}$-QD-$A647_{(25)}$; and (1, 1) $Tb_{(25)}$-QD-$A647_{(12)}$ (Figure 4a, c). The Select input refers to the time-delay in which PL is acquired. When select is "OFF" or "0", the PL intensity ratio from output A, A647(670 nm)/QD(625 nm) acquired 0 μs after excitation, is monitored at a threshold LT value of 1. Therefore the "OFF" select control input transmits the Boolean logic values from input B (0,0,1,1) to the output. When select is "ON", the PL intensity ratio from output B, A647(670 nm)/Tb(550 nm) acquired 55 μs after excitation, is monitored at a threshold LT

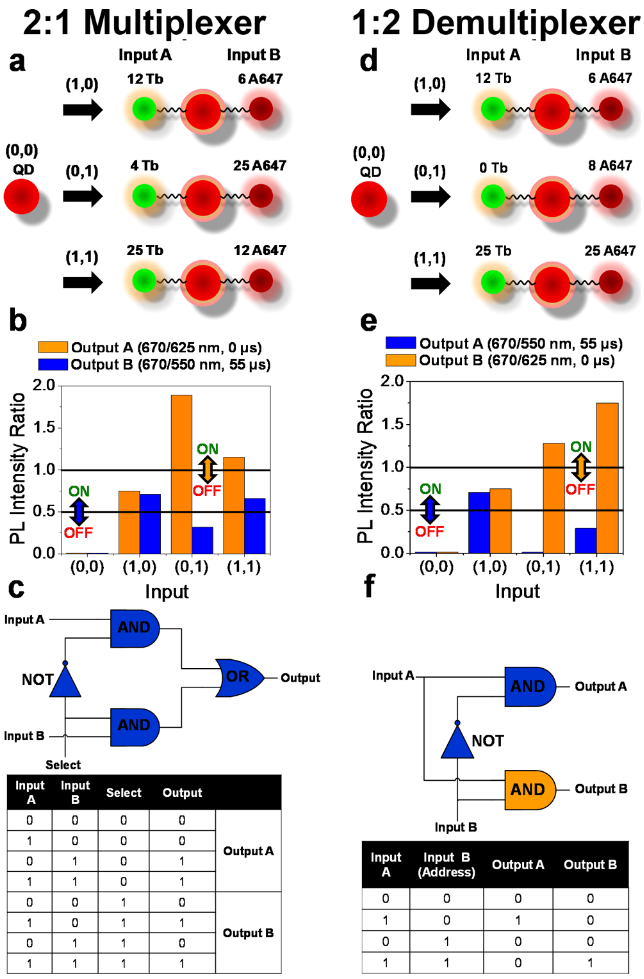

Input A	Input B	Select	Output	
0	0	0	0	Output A
1	0	0	0	
0	1	0	1	
1	1	0	1	
0	0	1	0	Output B
1	0	1	1	
0	1	1	0	
1	1	1	1	

Input A	Input B (Address)	Output A	Output B
0	0	0	0
1	0	1	0
0	1	0	0
1	1	0	1

Figure 4. Multiplexer and Demultiplexer. Molecular photonic (a−c) 2:1 multiplexer and (d−f) 1:2 demultiplexer displaying (a, d) the corresponding functional architecture with Tb (small green sphere) and A647 (small red sphere) valences around the QD (central red sphere) for each input. (b, e) Peak PL intensity ratio of A647(670 nm)/Tb(550 nm) in blue and the A647(670 nm)/QD(625 nm) ratio in orange acquired 55 μs (339 nm excitation) and 0 μs (400 nm excitation) after excitation, respectively, where the ratio above 0.5 or 1, respectively, is converted into the Boolean logic state of "ON or 1" and below as "OFF or 0". The corresponding (c, f) circuit diagrams and truth tables. Individual gates within the 1:2 Demultiplexer only are colored coded to coincide with the corresponding PL intensity ratios that they are generated from.

value of 0.5 and the Boolean logic values from Input A (0,1,0,1) are transmitted to the output. Thus, this photonic multiplexer is capable of combining two input signals or data streams into a signal data line.

Once incoming data streams have been merged into a single line through use of the 2:1 multiplexer, a "receiver" can then disentangle the conjoined data line into two distinct data streams via a 1:2 demultiplexer.[4,45] This permits data that have been merged and transmitted into a single data stream to be recovered again as separate, readable data lines. Our 1:2 demultiplexer is created by utilizing the following states for input A and input B: (0, 0) QD alone; (1, 0) $Tb_{(12)}$-QD-$A647_{(6)}$; (0, 1) $Tb_{(0)}$-QD-$A647_{(8)}$; and (1, 1) $Tb_{(25)}$-QD-$A647_{(25)}$ (Figure 4d, f). Input A acts as the incoming data stream while Input B acts as the enabler or address input. When the address input is "OFF" or "0", the Boolean logic from Input A is transmitted to output A, when it is "ON" or "1", input A is transmitted to output B (Figure 4f). Output A is created by monitoring the intensity ratio of A647(670 nm)/Tb(550 nm) 55 μs after 339 nm excitation while Output B monitors the ratio of A647(670 nm)/QD(625 nm) immediately after 400 nm excitation.

Keypad Lock. Finally, we created an all-photonic keypad lock; i.e., a unique class of logic that is only activated by specific sequences of photonic input signals or optical "passwords".[46] We utilize a preassembled $Tb_{(12)}$-QD-$A647_{(12)}$ system as our central processing unit, Figure 5, with these particular Tb-to-QD and A647-to-QD valences setting the combination of the lock. This lock builds upon previous photonic-based designs that utilized multiple UV excitation wavelengths or multi-wavelength emissions as primary inputs.[47−49] The keypad lock possesses two photonic inputs and one time-based input: 339 (339 nm excitation), 400 (400 nm excitation), and TG (time-delay of 55 μs). These three inputs need to be applied in the correct-sequential order to turn on the two PL intensity ratio outputs (i.e., output A/B) that subsequently open the lock (e.g., time-gated detection can only lead to a PL output if 339 nm excitation is performed before detection). The three inputs create 16 possible three-digit codes for "entering" by the user (Figure 5). The two outputs are obtained by monitoring the peak PL intensity ratios of A647(670 nm)/Tb(550 nm) and A647(670 nm)/QD(625 nm) ratio acquired at 55 and 0 μs, respectively, after excitation (Figure 5). To open the keypad lock, both outputs need to be turned "ON" meaning their PL intensity ratios have reached above their threshold values of 0.5 and 1, respectively. The keypad lock is only turned on when the three inputs are applied in the following order: 339, TG, and 400. This all-photonic based keypad lock design overcomes some drawbacks (e.g., diffusion limitations and limited gate life) of molecular keypad locks that use chemical inputs because it can be opened nearly instantaneously without chemical by-product formation during operation, potentially permitting rapid-continuous use.[50−52]

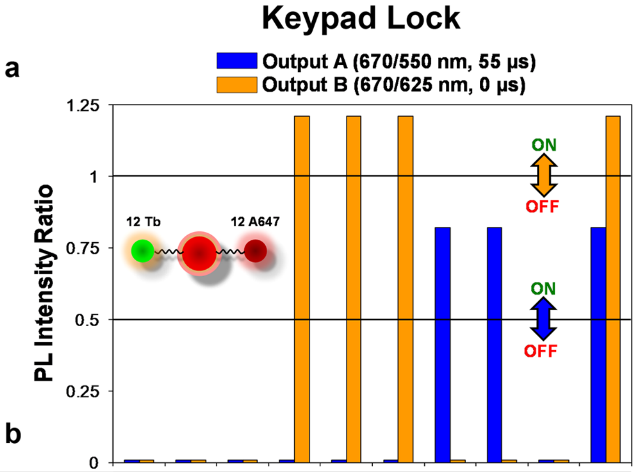

Code Sequence	1	2 3 4	5 6 7	8 9 10	11	12	13	14	15	16
1st Input	0	0 0 TG	0 0 339	0 0 400	TG	TG	339	400	400	339
2nd Input	0	0 TG 0	0 339 0	0 400 0	339	400	400	339	TG	TG
3rd Input	0	0 0 TG	339 0 0	400 0 0	400	339	TG	TG	339	400
Output A 670/550 nm	OFF	OFF	OFF	OFF	OFF	OFF	ON	ON	OFF	ON
Output B 670/625 nm	OFF	OFF	OFF	ON	ON	ON	OFF	OFF	OFF	ON
Keypad Lock	OFF	OFF	OFF	OFF	OFF	OFF	OFF	OFF	OFF	ON

Figure 5. Keypad Lock. Molecular keypad lock that is opened when only the correct input sequence (Input 1, Input 2, and Input 3) consisting of 339 nm excitation (339), a time-delay of 55 μs (TG), and 400 nm excitation with non-gated detection (400) is applied to a $Tb_{(12)}$-QD-$A647_{(12)}$ device. (a) The PL intensity ratio graph (670/550 nm in blue and 670/625 nm in orange) corresponding to the 3 input sequences and their permutations presented in the keypad lock table below. (b) Keypad lock table with the 16 possible three-digit codes that can be entered by the user: (1) no TG, no 339, no 400; (2−4) TG, no 339, and no 400 entered in three distinct combinations; (5−7) no TG, 339, and no 400 entered in three distinct combinations; (8−10) no TG, no 339, and 400 entered in three distinct combinations and sequential inputs of (11) TG, 339, 400; (12) TG, 400, 339; (13) 339, 400, TG; (14) 400, 339, TG; (15) 400, TG, and 339; and finally (16) the sequential input combination that opens the keypad lock is 339, TG, and 400.

4. CONCLUSIONS

This work demonstrates the computational richness of the three-luminophore Tb-QD-A647 system as a BLD. The inherent power stems from its time-dependent PL signatures that arise from the multi-FRET pathways which, in turn, are enabled by the Tb complex's ability to store the optical signal. This QD-based approach to BLD design produced complex combinatorial circuits (half-adder, half-subtractor, 2:1 multiplexer, 1:2 demultiplexer) and sequential logic (3-digit, 16-combination keypad lock). In all these applications, multiple gates are used, but are configured in parallel as a single stage so as to avoid the I/O incompatibility that seems inherent to MLDs. Our results demonstrate that both combinatorial and sequential logic can be developed solely from a single supramolecular assembly with all-photonic interrogation/output signals without requiring dynamic structural changes, mixed I/O signals (e.g., chemical and photonic), multicomponent biochemical heterostructures that required conformational changes, and/or dye excitation/monitoring at multiple different wavelengths. This may overcome, in part, the functional complexity and fabrication time/cost that has limited MLD utility in biological environments.

The three-luminophore Tb-QD-A647 system produces combinatorial arithmetic, multiplexer, and demultiplexer circuits that process four combinations of two input signals. The two input signals are the quantity of Tb (input A) and A647 (input B) co-assembled around the central quantum dot via peptides, PEP A and PEP B, that self-assemble on the QD surface driven by His_n metal affinity coordination (see

Experimental section). The converted PL ratios of the distinct Tb-QD-A647 bioconjugates for each state of the two input signals [i.e., (0, 0), (1, 0), (0, 1), and (1, 1)] is used as the logic output. This photonic emission is converted into Boolean logic outputs by monitoring discrete Tb, QD, or A647 PL intensity ratios in time-gated and non-time-gated modes after UV excitation at 339 nm and 400 nm, respectively. This allows us to further establish threshold "ON/OFF" or "1/0" lines (1 for non time-gated PL and 0.5 for time-gated PL). In the case of the half-adder, we can create the AND gate (carry term) and XOR gate (sum term) by monitoring the PL intensity ratio of identical Tb-QD-A647 bioconjugates in a non-time-gated and time-gated fashion. Likewise the 2:1 multiplexer and the 1:2 demultiplexer are constructed in a similar fashion where identical Tb and A647 inputs create two distinct logical outputs by monitoring PL intensity ratios in a non-time-gated and time-gated fashion. Conversely, the half-subtractor uses distinct Tb or A647 inputs to create the XOR gate (difference term) and INHIBIT gate (borrow term) by monitoring the different Tb-QD-A647 bioconjugates all in a time-gated fashion. For the 2:1 multiplexer, the time of PL acquisition also acts as a third input or "select" input. Furthermore, a sequential keypad lock that produces 16 unique combinations from three digits is also produced from the Tb-QD-A647 bioconjugates. However, the quantity of Tb and A647 co-assembled around the central QD here is held constant while the time of PL acquisition and magnitude of UV excitation acts as inputs and the correct order or sequence of these inputs opens the lock. Therefore logical "circuits" (i.e., the fusion of logical expressions from more than one logic gate) are expressed photonically via the Tb-QD-A647 supramolecules by manipulating both the quantity of Tb and A647 inputs and the time at which resultant PL is acquired.

In terms of applications, temporally-variant complex logic in a single device could potentially be used in cells or in vivo for sensing where multiphoton excitation can penetrate tissue, with the time-delayed PL acquisition significantly reducing background fluorescence interference.[53−55] For these purposes it would be important to implement the parallel gates using bioorthogonal chemistries,[56,57] so that they perform their function within the one "pot" environment that is a biological cell. The keypad lock, developed using an analogous strategy to that employed by ATM terminals for identification, is perhaps closer to implementation as it functions with minimal constraints because users need only input appropriate combinations of excitation wavelengths and PL capture time in order to open the lock. Such unconventional photonic and temporal inputs could decrease the forgery and cracking of systems that require sophisticated security.[58]

■ ASSOCIATED CONTENT

Ⓢ Supporting Information

PL emission plots corresponding to the half-adder, half-subtractor, 2:1 multiplexer, 1:2 demultiplexer, and keypad lock logic presented in Figures 3−5. This material is available free of charge via the Internet at http://pubs.acs.org.

■ AUTHOR INFORMATION

Corresponding Author

*E-mail: igor.medintz@nrl.navy.mil.

Notes

The authors declare no competing financial interest.

■ ACKNOWLEDGMENTS

The authors acknowledge the NRL NSI, ONR, DTRA-JSTO MIPR No. B112582M for financial support; Lumiphore, Inc. for the Lumi4-Tb reagents; and Invitrogen Life Sciences for the QDs.

■ REFERENCES

(1) de Silva, P. A.; Gunaratne, N. H. Q.; McCoy, C. P. *Nature* **1993**, *364*, 42−44.

(2) de Silva, A. P.; Uchiyama, S. *Nat. Nanotechnol.* **2007**, *2*, 399−410.

(3) Credi, A.; Balzani, V.; Langford, S. J.; Stoddart, J. F. *J. Am. Chem. Soc.* **1997**, *119*, 2679−2681.

(4) Andréaasson, J.; Gust, D. In *Molecular and Supramolecular Information Processing: From Molecular Switches to Logic Systems*, 1st ed.; Katz, E., Ed.; Wiley-VCH: Weinheim, Germany, 2012; Chapter 4, p 53.

(5) Andreasson, J.; Pischel, U. *Chem. Soc. Rev.* **2010**, *39*, 174−188.

(6) Zhai, Y.; Zhu, Z.; Zhu, C.; Zhu, J.; Ren, J.; Wang, E.; Dong, S. *Nanoscale* **2013**, *5*, 4344−4350.

(7) Auslander, S.; Auslander, D.; Muller, M.; Wieland, M.; Fussenegger, M. *Nature* **2012**, *487*, 123−127.

(8) Yang, J.; Shen, L.; Ma, J.; Schlaberg, H. I.; Liu, S.; Xu, J.; Zhang, C. *ACS Appl. Mater. Interfaces* **2013**, *5*, 5392−5396.

(9) Privman, M.; Tam, T. K.; Bocharova, V.; Halámek, J.; Wang, J.; Katz, E. *ACS Appl. Mater. Interfaces* **2011**, *3*, 1620−1623.

(10) Motornov, M.; Zhou, J.; Pita, M.; Gopishetty, V.; Tokarev, I.; Katz, E.; Minko, S. *Nano Lett.* **2008**, *8*, 2993−2997.

(11) Manesh, K. M.; Halámek, J.; Pita, M.; Zhou, J.; Tam, T. K.; Santhosh, P.; Chuang, M.-C.; Windmiller, J. R.; Abidin, D.; Katz, E. *Biosens. Bioelectron.* **2009**, *24*, 3569−3574.

(12) Katz, E.; Bocharova, V.; Privman, M. *J. Mater. Chem.* **2012**, *22*, 8171−8178.

(13) Elbaz, J.; Willner, I. *Nat. Mater.* **2012**, *11*, 276−277.

(14) Graugnard, E.; Kellis, D. L.; Bui, H.; Barnes, S.; Kuang, W.; Lee, J.; Hughes, W. L.; Knowlton, W. B.; Yurke, B. *Nano Lett.* **2012**, *12*, 2117−2122.

(15) Konry, T.; Walt, D. R. *J. Am. Chem. Soc.* **2009**, *131*, 13232−13233.

(16) Qu, D. H.; Wang, Q. C.; Tian, H. *Angew. Chem., Int. Ed.* **2005**, *44*, 5296−5299.

(17) Saghatelian, A.; Volcker, N. H.; Guckian, K. M.; Lin, V. S. Y.; Ghadiri, M. R. *J. Am. Chem. Soc.* **2002**, *125*, 346−347.

(18) Melnikov, D.; Strack, G.; Zhou, J.; Windmiller, J. R.; Halámek, J.; Bocharova, V.; Chuang, M.-C.; Santhosh, P.; Privman, V.; Wang, J. *J. Phys. Chem. B* **2010**, *114*, 12166−12174.

(19) Katz, E.; Wang, J.; Privman, M.; Halámek, J. *Anal. Chem.* **2012**, *84*, 5463−5469.

(20) Algar, W. R.; Malanoski, A. P.; Susumu, K.; Stewart, M. H.; Hildebrandt, N.; Medintz, I.L. *Anal. Chem.* **2012**, *84*, 10136−10146.

(21) Algar, W. R.; Wegner, D.; Huston, A. L.; Blanco-Canosa, J. B.; Stewart, M. H.; Armstrong, A.; Dawson, P. E.; Hildebrandt, N.; Medintz, I. L. *J. Am. Chem. Soc.* **2012**, *134*, 1876−1891.

(22) Claussen, J. C.; Algar, W. R.; Hildebrandt, N.; Susumu, K.; Ancona, M. G.; Medintz, I. L. *Nanoscale* **2013**, *5*, 12156−12170.

(23) Algar, W. R.; Susumu, K.; Delehanty, J. B.; Medintz, I. L. *Anal. Chem.* **2011**, *83*, 8826−8837.

(24) Petryayeva, E.; Medintz, I. L.; Algar, W. R. *Appl.Spect.* **2013**, *67*, 215−252.

(25) Algar, W. R.; Kim, H.; Medintz, I. L.; Hildebrandt, N. *Coord. Chem. Rev.* **2013**, in press; http://dx.doi.org/10.1016/j.ccr.2013.07.015.

(26) Credi, A. *New J. Chem.* **2012**, *36*, 1925−1930.

(27) Hötzer, B.; Medintz, I. L.; Hildebrandt, N. *Small* **2012**, *8*, 2297−2326.

(28) Geißler, D.; Lindén, S.; Liermann, K.; Wegner, K. D.; Charbonnière, L. J.; Hildebrandt, N. *Inorg. Chem.* 2013, *In Press*, DOI: 10.1021/ic4017883.

(29) Geißler, D.; Stufler, S.; Löhmannsröben, H.-G.; Hildebrandt, N. *J. Am. Chem. Soc.* **2013**, *135*, 1102−1109.

(30) Geißler, D.; Charbonnière, L. J.; Ziessel, R. F.; Butlin, N. G.; Löhmannsröben, H.-G.; Hildebrandt, N. *Angew. Chem. Int. Ed.* **2010**, *49*, 1396−1401.

(31) Li, J.; Li, X.; Shi, X.; He, X.; Wei, W.; Ma, N.; Chen, H. *ACS Appl. Mater. Interfaces* **2013**, *5*, 9798−9802.

(32) Sapsford, K. E.; Farrell, D.; Sun, S.; Rasooly, A.; Mattoussi, H.; Medintz, I. L. *Sens. Actuators, B* **2009**, *139*, 13−21.

(33) Susumu, K.; Oh, E.; Delehanty, J. B.; Blanco-Canosa, J. B.; Johnson, B. J.; Jain, V.; Hervey, W. J.; Algar, W. R.; Boeneman, K.; Dawson, P. E.; Medintz, I. L. *J. Am. Chem. Soc.* **2011**, *133*, 9480−9496.

(34) Mei, B. C.; Susumu, K.; Medintz, I. L.; Mattoussi, H. *Nat. Protoc.* **2009**, *4*, 412−423.

(35) Mei, B. C.; Susumu, K.; Medintz, I. L.; Delehanty, J. B.; Mountziaris, T. J.; Mattoussi, H. *J. Mat. Chem.* **2008**, *18*, 4949−4958.

(36) Sapsford, K. E.; Pons, T.; Medintz, I. L.; Higashiya, S.; Brunel, F. M.; Dawson, P. E.; Mattoussi, H. *J. Phys. Chem. C* **2007**, *111*, 11528−11538.

(37) Sapsford, K. E.; Algar, W. R.; Berti, L.; Boeneman Gemmill, K.; Casey, B. J.; Oh, E.; Stewart, M. H.; Medintz, I. L. *Chem. Rev.* **2013**, *113*, 1904−2074.

(38) Prasuhn, D. E.; Deschamps, J. R.; Susumu, K.; Stewart, M. H.; Boeneman, K.; Blanco-Canosa, J. B.; Dawson, P. E.; Medintz, I. L. *Small* **2010**, *6*, 555−564.

(39) Blanco-Canosa, J.; Wu, M.; Susumu, K.; Petryayeva, E.; Jennings, T. L.; Dawson, P. E.; Algar, W. R.; Medintz, I. L. *Coord. Chem. Rev.* **2013**, in press; http://dx.doi.org/10.1016/j.ccr.2013.08.030.

(40) Prasuhn, D.E.; Blanco-Canosa, J.B.; Vora, G.J.; Delehanty, J.B.; Susumu, K.; Mei, B.C.; Dawson, P.E.; Medintz, I. L. *ACS Nano* **2010**, *4*, 267−278.

(41) Boeneman, K.; Deschamps, J.R.; Buckout-White, S.; Prasuhn, D.E.; Blanco-Canosa, J.B.; Dawson, P.E.; Stewart, M.H.; Susumu, K.; Goldman, E.R.; Ancona, M.; Medintz, I. L. *ACS Nano* **2010**, *4*, 7253−7266.

(42) Wegner, K. D.; Lanh, P. T.; Jennings, T.; Oh, E.; Jain, V.; Fairclough, S. M.; Smith, J. M.; Giovanelli, E.; Lequeux, N.; Pons, T.; Hildebrandt, N. *ACS Appl. Mater. Interfaces* **2013**, *5*, 2881−2892.

(43) Park, K. S.; Seo, M. W.; Jung, C.; Lee, J. Y.; Park, H. G. *Small* **2012**, *8*, 2203−2212.

(44) Straight, S. D.; Liddell, P. A.; Terazono, Y.; Moore, T. A.; Moore, A. L.; Gust, D. *Adv. Funct. Mater.* **2007**, *17*, 777−785.

(45) Andréasson, J.; Pischel, U.; Straight, S. D.; Moore, T. A.; Moore, A. L.; Gust, D. *J. Am. Chem. Soc.* **2011**, *133*, 11641−11648.

(46) Rout, B.; Milko, P.; Iron, M. A.; Motiei, L.; Margulies, D. *J. Am. Chem. Soc.* **2013**, *135*, 15330−15333.

(47) Guo, J.; Ju, J.; Turro, N. J. *Anal. Bioanal.Chem.* **2012**, 1−11.

(48) Angelos, S.; Yang, Y. W.; Khashab, N. M.; Stoddart, J. F.; Zink, J. I. *J. Am. Chem. Soc.* **2009**, *131*, 11344−11346.

(49) Andreasson, J.; Straight, S. D.; Moore, T. A.; Moore, A. L.; Gust, D. *Chem.—Eur. J.* **2009**, *15*, 3936−3939.

(50) Pischel, U.; Andreasson, J. *New J. Chem.* **2010**, *34*, 2701−2703.

(51) Suresh, M.; Ghosh, A.; Das, A. *Chem. Commun.* **2008**, 3906−3908.

(52) Sun, W.; Zhou, C.; Xu, C. H.; Fang, C. J.; Zhang, C.; Li, Z. X.; Yan, C. H. *Chem.—Eur. J.* **2008**, *14*, 6342−6351.

(53) Clapp, A. R.; Pons, T.; Medintz, I. L.; Delehanty, J. B.; Melinger, J. S.; Tiefenbrunn, T.; Dawson, P. E.; Fisher, B. R.; O'Rourke, B.; Mattoussi, H. *Adv. Mater.* **2007**, *19*, 1921−1926.

(54) Morgner, F.; Stufler, S.; Geißler, D.; Medintz, I. L.; Algar, W. R.; Susumu, K.; Stewart, M. H.; Blanco-Canosa, J. B.; Dawson, P. E.; Hildebrandt, N. *Sensors* **2011**, *11*, 9667−9684.

(55) Oh, E.; Fatemi, F. K.; Currie, M.; Delehanty, J. B.; Pons, T.; Fragola, A.; Leveque-Fort, S.; Goswami, R.; Susumu, K.; Huston, A. L.; Medintz, I. L. *Part. Part. Syst. Charact.* **2013**, *30*, 453−466.

(56) Sapsford, K.E.; Algar, W.R.; Berti, L.; Gemmill, K.B.; Casey, B.J.; Oh, E.; Stewart, M.H.; Medintz, I.L. *Chem. Rev.* **2013**, *113*, 1904−2074.

(57) Algar, W. R.; Prasuhn, D.E.; Stewart, M. H.; Jennings, T.L.; Blanco-Canosa, J.B.; Dawson, P.E.; Medintz, I. L. *Bioconjugate Chem.* **2011**, *18*, 825−858.

(58) Margulies, D.; Felder, C. E.; Melman, G.; Shanzer, A. *J. Am. Chem. Soc.* **2007**, *129*, 347−354.